Photochemical Mechanisms in Atmospherically-Relevant Iodine Oxide Clusters

Nicoline C. Frederiks[a] and Christopher J. Johnson[a*]

[a] *Department of Chemistry, Stony Brook University, 100 Nicolls Rd., Stony Brook, NY 11794, United States*

E-mail: chris.johnson@stonybrook.edu

Abstract

Atmospheric new particle formation (NPF) events can be driven by iodine oxides or oxoacids via both neutral and ionic mechanisms. Photolysis of new particles likely plays a significant role in their growth mechanisms, but their spectra and their photolysis mechanisms remain difficult to characterize. We recorded UV photodissociation spectra of $(I_2O_5)_{0-3}(IO_3^-)$ clusters, observing loss of O atom, I_2O_4, and $(I_2O_5)_{1,2}$ in the atmospherically-relevant range 300-340 nm. With increasing cluster size, absorption red shifts and generally increases in intensity, suggesting particles photolyze more frequently as they grow. Estimates of the rates indicate that even relatively small clusters are likely to undergo photolysis in ambient conditions. Vibrational spectra identify the covalent moiety $I_3O_8^-$ as the likely chromophore, not IO_3^-. The I_2O_5-loss pathway competes with particle growth while the slower O loss pathway likely produces ^{3}O + ^{3}(cluster) products that could drive subsequent intra-particle chemistry, particularly with co-adsorbed organic or amine species.

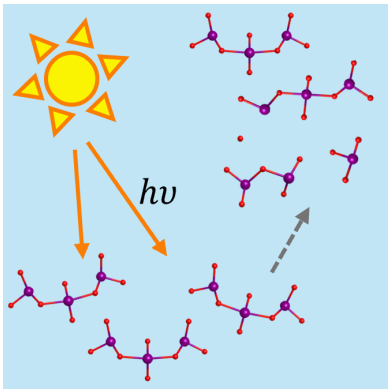

New particle formation (NPF) is the process by which trace atmospheric gases cluster together and, under specific conditions, grow to become secondary aerosol particles via condensation of gases and/or coagulation with other atmospheric particles and small clusters.[1–3] These secondary aerosol particles can directly and indirectly influence the radiative forcing balance of the atmosphere by scattering radiation and seeding clouds, ultimately impacting the current and future climate.[4,5] Ammonia and sulfuric acid containing clusters are the most well studied NPF clusters to date,[6–14] having been observed in many field campaigns[15–17] as they form from direct (NH_3) and indirect (SO_2 reacting to form H_2SO_4)[18] post-industrial-revolution anthropogenic emissions.[19]

Studies performed in coastal mid-latitude and polar regions have uncovered the importance iodine plays in NPF.[20–24] I_2 and organo-iodide molecules such as CH_3I[20,25,26] and CH_2I_2[27–30] are introduced into the atmosphere via several pathways, including: directly from oceanic biota (such as algae),[25,27,31,32] from ocean surface reactions,[33–36] and from snow pack and ice brine evaporation.[30,37,38] In the poles, photolysis of snow packs and ice plays a key role in increasing gas phase atmospheric iodine concentrations during daylight hours.[30,38] In the coastal mid-latitude regions during daytime at low tide, a large source of iodine species is believed to stem from photooxidation of freshly exposed oceanic biota.[28] I_2 undergoes photolysis on the order of 5-10 s as it absorbs sunlight wavelengths of 400-700 nm,[39] whereas CH_2I_2 likely only undergoes photolysis on the order of 12 min to 13 hrs[40] as it primarily absorbs in the 300-350 nm range.[41] I atoms can react very efficiently with tropospheric O_3 to form IO,[21,42–44] with reported polar springtime tropospheric ozone depletion events of 15-30 ppb, which was predominantly attributed to iodine.[38] IO can further undergo photolysis or react with other gas phase species to form larger iodine oxides.[45–47] These somewhat larger iodine oxides encounter a similarly competitive fate, where photolysis leads to recycling of atmospheric iodine, but gas phase reactions can result in larger iodine oxide molecule formation which can potentially grow into iodine oxide particles (IOPs).[48,49]

Several studies have examined photodissociation of iodine oxide molecules including

IO,[22,43,50–55] OIO,[43,51,52,56–60] and I_2O_{2-3},[61] along with kinetics/rates of these photolysis reactions.[62–64] Larger iodine oxides ($I_{2-5}O_{2-12}$) have also been studied, probing photolysis reaction rates and their absorption cross sections, and photolysis reactions for iodate have been proposed.[65,66] Some of these iodine oxide molecules, such as I_2O_3, have small enough absorption cross sections in the actinic region that they likely live long enough to play a role in NPF and clustering.[66] IOP formation appears to be driven by temperature and humidity: under cooler, drier conditions I_2O_3 and I_2O_4 are found to polymerize into larger and more abundant IOPs.[67] A further study concluded I_2O_4 is the most likely of the smaller iodine oxide molecules to initiate NPF, with some likely contribution from I_2O_5.[68] Yet another study identified the presence of I_2O_5 in IOP nanoparticles concluding that IOPs formed in coastal marine boundary layers are likely made up of I_2O_5.[69]

Anionic species are expected to be important in iodine-driven NPF. Chamber experiments found that ion-induced nucleation driven by IO_3^- was efficient, and suggested that in some conditions it may be the dominant mechanism.[70] Observed clusters generally followed the pattern $(I_2O_5)_{0-7}(HIO_3)_{0-1}(IO_{1-3}^-)$. Although neutrals are more abundant, anionic clusters have been found to be more stable against dissociation by ion mobility-mass spectrometry (IM-MS) during field observations, indicating these clusters could grow more quickly in the atmosphere.[71] They are also directly observed in ambient sampling and chemical ionization mass spectrometry experiments, though the degree to which nitrate chemical ionization faithfully preserves the composition of new particles has been questioned.[72] Furthermore, mixed IOP containing iodic acid and any less acidic species are likely to deprotonate iodic acid, and clusters including sulfuric acid and ammonia have been observed.[73,74] Thus, these anionic clusters can also be viewed as likely subunits of larger pure or mixed IOPs. Despite the findings suggesting full conversion of I_2O_5 to HIO_3 even at relative humidities below 65%,[71] another study determined clustering of iodine oxides was still the primary IOP formation pathway even at high relative humidities.[47]

Here we use mass-resolved gas phase ultraviolet (UV) spectroscopy, and infrared (IR)

spectroscopy to examine how likely and to what extent photolysis impacts iodine oxide NPF clusters of the following composition $(I_2O_5)_{0-4}(IO_3^-)$. Performing spectroscopy directly on mass selected ions gives the ability to explicitly link photolysis products to specific cluster compositions and absorption wavelengths, giving direct insight into elementary photolysis mechanisms. The experimental procedure is described in the Experimental Methods section.

While IO_3^- only shows significant absorption well into the deep UV, we find that clustering with I_2O_5 results in absorption at atmospherically relevant wavelengths. Figure 1 displays survey spectra of IO_3^-, $(I_2O_5)(IO_3^-)$, $(I_2O_5)_4(IO_3^-)$, and $(I_2O_5)_8(IO_3^-)_2$ from 250-340 nm, recorded by monitoring loss of O atoms upon irradiation of all clusters simultaneously while stored in an ion trap. We have also overlaid the AM1.5G reference solar irradiance spectrum[75] (in orange) to identify the atmospherically relevant region of the experimental spectra, which is highlighted by the yellow structure in Figure 1. Diffuse and scattered light is included in the spectrum, and an air mass coefficient of 1.5 corresponds to a solar zenith angle of 48.2°, located at sea level in the mid-latitudes. UV light below 290 nm is efficiently filtered by stratospheric ozone, so only absorption beyond 290 nm will potentially impact NPF.

Analyzing the photolysis spectra, we see a very weak absorption for IO_3^- that is too deep into the UV to be atmospherically relevant, with only negligible absorption above 300 nm. However, the larger clusters show more notable absorption in the atmospherically-relevant window. The smallest cluster, $(I_2O_5)(IO_3^-)$, displays the highest peak intensity overall, but relatively weak absorption above 300 nm. Larger clusters continue to show red shifts of these absorption features. $(I_2O_5)_4(IO_3^-)$, despite absorbing more weakly in the deep UV, shows stronger absorption at longer wavelengths, with the doubly charged $(I_2O_5)_8(IO_3^-)$ cluster absorbing well beyond 320 nm. This suggests that increasing cluster size via units of I_2O_5 shifts photolysis into the atmospherically relevant wavelengths.

We then sought to survey a broad range of clusters to determine the prevalence of this photolysis mechanism. We recorded a series of mass spectra in the mass range of 30-2060

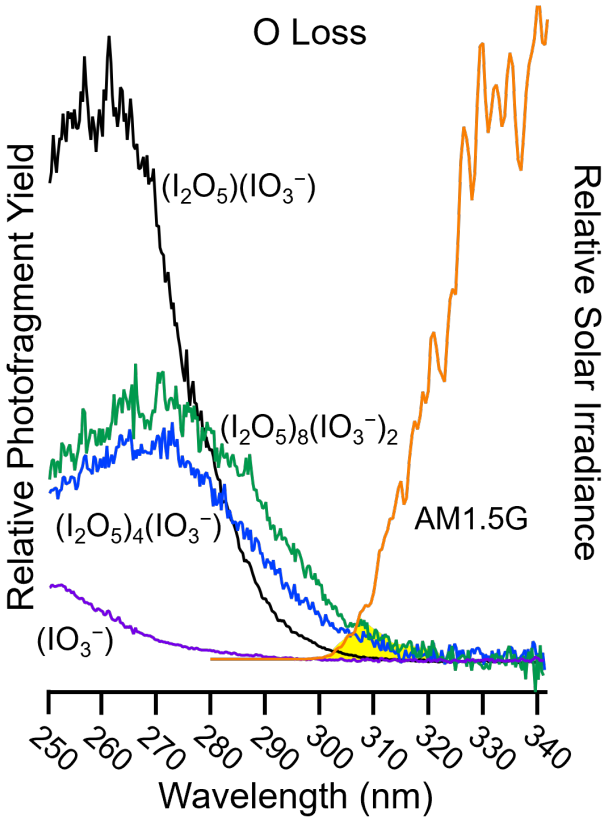

Figure 1: O-loss UV photofragmentation spectra of IO_3^-, $(I_2O_5)(IO_3^-)$, $(I_2O_5)_4(IO_3^-)$, and $(I_2O_5)_8(IO_3^-)_2$ compared to the standard solar spectrum AM1.5G are depicted. The yellow area highlighted between the two sets of spectra displays the region of overlap of atmospherically relevant wavelengths with the UV cluster spectra. Absorption shifts into the atmospherically-relevant window as cluster size increases.

m/z, with and without 300 nm laser light. Figure 2 shows a plot of difference mass spectra for absorption at 300 nm, calculated by subtracting the steady state mass spectrum with the laser on from that when the laser is blocked. The positive intensities, therefore, identify cluster compositions with increased population upon 300 nm irradiation and the negative intensities establish clusters that are depleted. Artifacts resulting from changes in peak shape are noted by a red *. All clusters of the composition $(I_2O_5)_{n>1}(IO_3^-)$ appear to undergo fragmentation upon exposure to UV light. However, $I_2O_4(I_2O_5)_{n\geq1}(IO_3^-)$ cluster yields, representing the O loss channel from the $(I_2O_5)_{n>1}(IO_3^-)$ clusters, are not enhanced proportionally to the depletion of the parent, consistent with the coexistence of fragmentation channels yielding loss of $(I_2O_5)_{n\geq1}$. The positive IO_4^- fragment intensity in Figure 2 indicates I_2O_4 loss from the $(I_2O_5)(IO_3^-)$ cluster. Recording spectra in this manner makes it difficult to directly observe the (I_2O_5)-loss channel, necessitating an alternate experimental modality.

In order to quantify the relative yields of the O loss and I_2O_5 loss channels, we instead recorded spectra by mass selecting a single cluster composition by linear time of flight mass spectrometry, irradiating it with a tunable laser pulse, and mass separating the fragments by reflectron time of flight mass spectrometry. The spectra collected in this manner are displayed in Figure 3 for the following clusters: $(I_2O_5)(IO_3^-)$, $(I_2O_5)_2(IO_3^-)$, and $(I_2O_5)_3(IO_3^-)$. In all cases, we find that fragmentation results in more I_2O_5 loss than O loss by roughly a factor of 10. For $(I_2O_5)(IO_3^-)$, absorption occurs up to approximately 320 nm, regardless of photolysis product. Photolysis of $(I_2O_5)_2(IO_3^-)$ to produce I_2O_5 occurs up to 340 nm, while loss of O is not apparent beyond 320 nm. There are three distinct product channels detected for $(I_2O_5)_3(IO_3^-)$: loss of O, I_2O_5, and $(I_2O_5)_2$, each with an apparent maximum absorption wavelength of 325 nm. However, it is impossible to identify whether the latter results from loss of $2I_2O_5$ or I_4O_{10}.

While quantification of the absolute photolysis rates is difficult in the current experimental setup, we present conservative lower limits to these rates in Table 1 only to estimate the degree to which photochemistry of this type is likely to be relevant to NPF. More careful

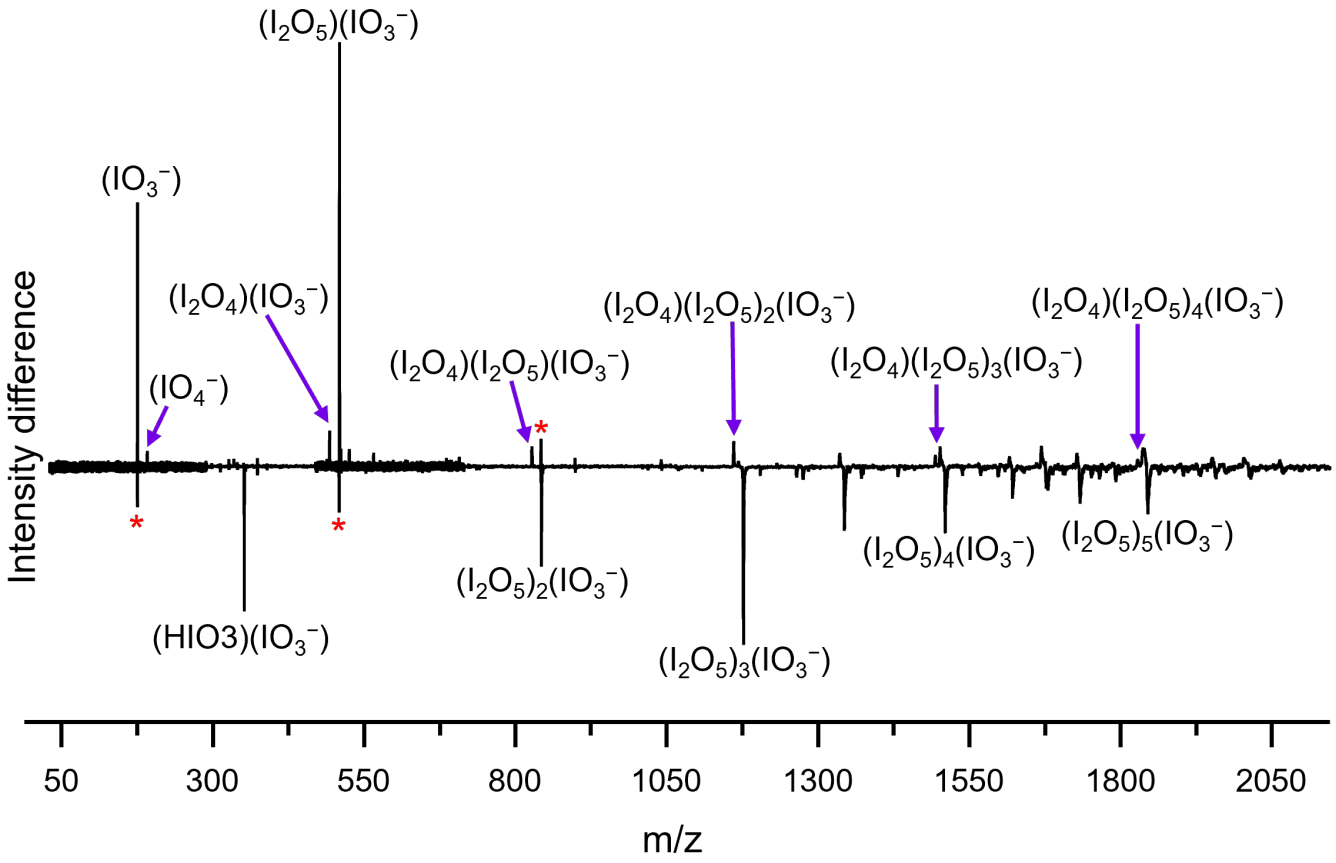

Figure 2: The difference mass spectra computed by subtracting a mass spectrum with no laser light shining on the clusters from a mass spectrum where the clusters were irradiated by 300 nm light. Positive intensities, therefore, represent clusters or fragments whose intensity increased upon exposure to 300 nm light and negative intensities signify clusters that fragmented when irradiated with 300 nm light. Peaks labeled by a red $*$ identify artifacts that resulted from the subtraction process due to small changes in peak shape and are not representative of an actual loss or gain in cluster/fragment intensity.

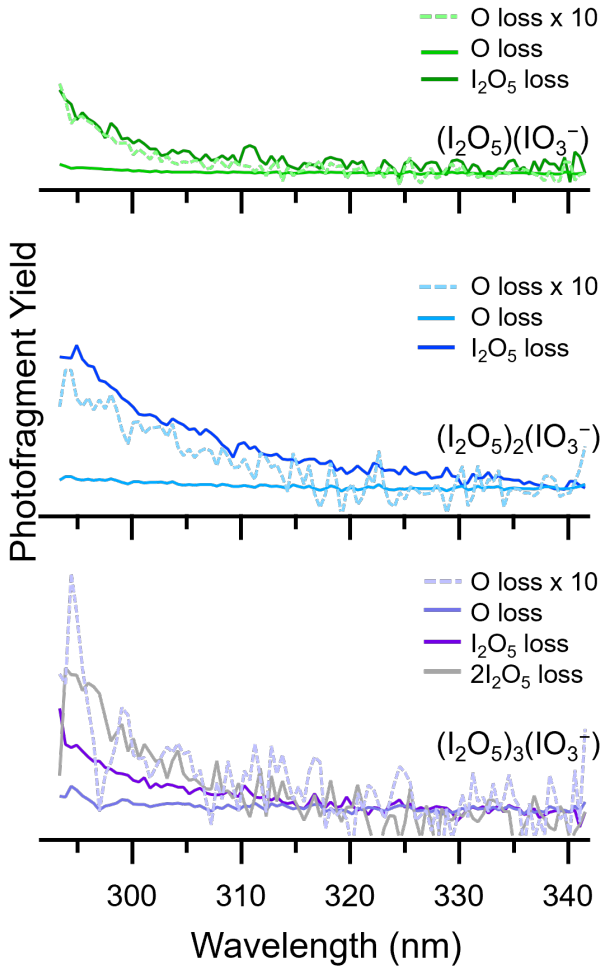

Figure 3: Spectra monitoring O loss and I_2O_5 loss for clusters of the composition $(I_2O_5)_{1-3}(IO_3^-)$ are displayed here. Both I_2O_5 loss and O loss absorption increases in intensity and range of absorption with increasing cluster size, though I_2O_5 loss is more prevalent.

kinetic measurements would be required to establish quantitative rates that could be incorporated into models. The calculation of these rates is described in the Supplementary Information, but briefly, we integrated the product of the experimental fragment yields (divided by photon flux) and the AM1.5G solar spectrum. Fragment yields are scaled to the O-loss fragment yield for $(I_2O_5)_2(IO_3^-)$, which was recorded with high signal to noise. We expect these rates to be lower bounds to the atmospheric rates because the AM1.5G reference spectrum is intended to represent a "typical" day in a terrestrial mid-latitude location at sea level. On a high-UV, low-ozone day in tropical coastal regions at altitude, the observed rates for clusters such as these are likely to be significantly higher, possibly by an order of magnitude. More sophisticated models to predict solar irradiance are available, but given the large experimental uncertainties in these measurements, we chose to simplify our analysis. Particularly due to the large contribution of baseline noise to the total integral at longer (higher UV flux) wavelengths, we anticipate relative uncertainties of 25% and absolute uncertainties of 50%.

Table 1: Estimates of the lower limits of photolysis rates for fragmentation by loss of O, I_2O_5, or $2I_2O_5$ under irradiation from the AM1.5G solar spectrum.

Cluster	O loss rate (s^{-1})	I_2O_5 loss rate (s^{-1})	$2I_2O_5$ loss rate (s^{-1})
IO_3^-	6×10^{-6}		
$(I_2O_5)(IO_3^-)$	$1.4 \times 10{-}4$	1.2×10^{-3}	
$(I_2O_5)_2(IO_3^-)$	2.6×10^{-4}	7.4×10^{-3}	
$(I_2O_5)_3(IO_3^-)$	5.4×10^{-4}	3.7×10^{-3}	5.8×10^{-3}

Analyzing the results, it is likely that photolysis of IO_3^- to yield loss of oxygen is too slow to significantly alter NPF mechanisms at any plausible UV solar irradiance. For clusters, we see photolysis by O loss to increase at least linearly with addition of I_2O_5, and on a high-UV day, O loss from $(I_2O_5)_3(IO_3^-)$ and larger clusters could be expected to occur in a matter of minutes. In all cases, photolysis yielding I_2O_5 is roughly an order of magnitude faster than loss of O. This process would simply compete with uptake of I_2O_5, while loss of O atoms will

qualitatively change the chemistry of the nascent particle. These rates are of similar orders of magnitude to those presented for smaller iodine oxides,[66] suggesting that photochemistry in more complex mixed new particles is likely to continue to be relevant.

Next, we sought to determine the nature of the chromophore responsible for UV absorption. We recorded vibrational spectra of the clusters $(I_2O_5)_{1-3}(IO_3^-)$ using cryogenic ion vibrational presdissociation spectroscopy (CIVP).[76] CIVP spectroscopy allows the vibrational spectra of clusters with specific compositions to be recorded. Thus, it is possible to establish experimentally present structures by comparing quantum-chemically-computed vibrational spectra for a number of structures to the experimental spectra. The experimental spectra are shown in black, and the computed spectra for the lowest energy isomers are shown in grey in Figure 4. The approach to generate the computed spectra was validated previously for clusters of this type[74] and is described in the Experimental Methods. The lowest energy optimized structures are shown alongside their corresponding computed spectra and their 0 K, zero-point-corrected internal energies. We explored previously reported structures of these cluster compositions[71] as well as derivatives of ones we previously reported[74] as a starting point for structure generation. Further candidate structures were developed using chemical intuition, and all were optimized to local minima. While this approach does not exhaustively explore the structural space available to these clusters, it is sufficient to identify the structural motif associated with the UV chromophore.

For the $(I_2O_5)(IO_3^-)$ cluster, we find two nearly isoenergetic structures. The computed spectrum of isomer 1a shows very good agreement with the experimental spectrum, reproducing the three peaks in the 800-900 cm^{-1} range nearly quantitatively. It also captures the position of the peak near 700 cm^{-1} accurately. The intensity of this peak is likely suppressed in the experimental spectrum due to the binding energy of the N_2 adduct. This binding energy is typically ~800 cm^{-1}, so a single photon of less than 800 cm^{-1} is not always sufficient to induce tag dissociation. The spectrum of isomer 1c[71] is also broadly consistent with the experimental spectrum, but the relative intensity patterns and peak positions in the 800-900

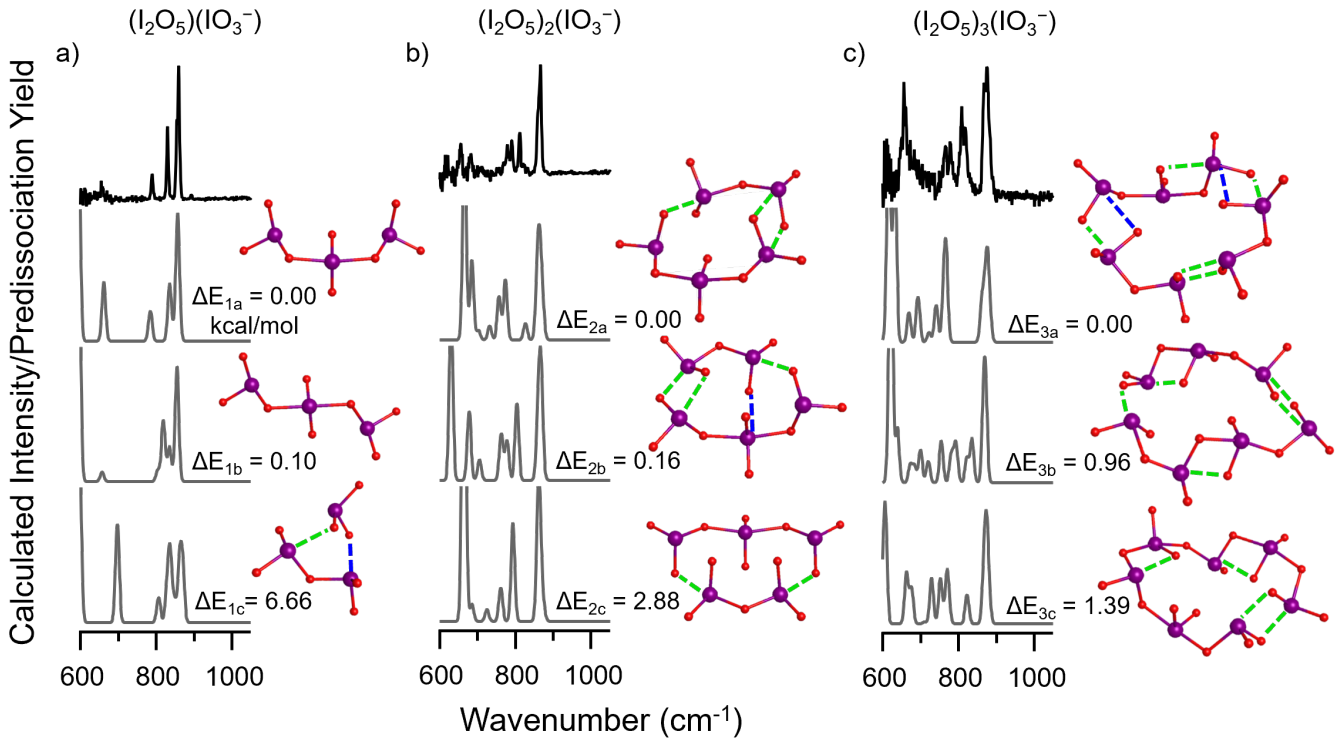

Figure 4: A comparison of the experimental IR spectra of a) $(I_2O_5)(IO_3^-)$, b) $(I_2O_5)_2(IO_3^-)$, and c) $(I_2O_5)_3(IO_3^-)$ versus their lowest three energy computed spectra. All relative energies are reported in kcal/mol. Structure 1c has been reported before in a previous study.[71] We assign structures 1a and 2b as the experimentally-present structures. None of the current computed spectra satisfactorily replicate the experimentally present one, but similarities between the experimental spectra of $(I_2O_5)_2(IO_3^-)$ and $(I_2O_5)_3(IO_3^-)$ suggest comparable structures for these clusters.

cm^{-1} range display a worse match than Isomer 1a. Isomer 1c is also significantly higher in energy; as a result we do not expect it to be present in the experiment.

Moving to the next bigger cluster, $(I_2O_5)_2(IO_3^-)$, we identify the second lowest energy structure, 2b, as the most likely experimentally present structure. Although it is slightly higher in energy than isomer 1a, the energy difference is still within the expected uncertainty of the calculation. It best reproduces the doublet-singlet pattern found around 800 cm^{-1} in the experimental spectrum as well as the spacing of the three peaks below 700 cm^{-1}. Again, we expect the relative intensities of the peaks below 700 cm^{-1} to be suppressed in the experimental spectra due to N_2 binding energy.

In both of these assigned clusters, it is apparent from the structures that an $I_3O_8^-$ molecule is present. We previously showed that a covalently-bound $I_3O_8^-$ forms in cationic clusters consisting of ammonia, iodic acid, and iodine pentoxide.[74] This suggests that the actual composition of these clusters is best described as $(I_3O_8^-)$ and $(I_3O_8^-)(I_2O_5)$ rather than $(I_2O_5)(IO_3^-)$ and $(I_2O_5)_2(IO_3^-)$, respectively. These structural assignments lead us to conclude that $I_3O_8^-$ is the UV chromophore driving the photochemistry discussed above. The absorption of IO_3^- is weak and shifted well into atmospherically-irrelevant range of the UV near 260 nm, while $I_3O_8^-$ and $(I_3O_8^-)(I_2O_5)$ absorb strongly and with notable intensity above 300 nm.

None of the calculations for $(I_2O_5)_3(IO_3^-)$ capture the experimental spectrum satisfactorily. Given the size and complexity of the cluster, identification of the global minimum structure is a significant challenge. Nonetheless, comparison of the experimental spectrum of $(I_2O_5)_3(IO_3^-)$ and $(I_2O_5)_2(IO_3^-)$ shows striking similarities, particularly with respect to the peaks between 750-850 cm^{-1}, suggesting structural similarities. Analyzing the two lowest energy computed structures, we again find an $I_3O_8^-$ moiety, and in the slightly higher energy structure a single fully covalently-bound structure can be found. These two pieces of evidence suggest that $I_3O_8^-$ remains a structural feature of this cluster and continues to drive photolysis.

Next, we aimed to understand the photolysis mechanism, mainly 1.) whether dissociation

happens on the ground or excited electronic states, and 2.) whether it produces triplet or singlet oxygen. We first performed collision induced dissociation (CID) mass spectrometry experiments on these clusters using a Thermo Scientific LTQ XL ion trap mass spectrometer (Figures S1-S5). CID experiments are expected to drive fragmentation via a ground state mechanism, thermal decomposition. In all cases we observe decomposition by loss of I_2O_5 molecules, with no evidence of loss of O atoms. We cannot rule out the possibility that O atom loss occurs on a very hot ground state resulting from internal conversion, but the CID results suggest that O atom loss occurs through an excited state mechanism. However, it does not allow us to determine whether it results from direct photodissocation or from more complex excited state dynamics.

Finally, we focused on identifying whether O atom fragmentation yields ^{1}O or ^{3}O, and by extension, a singlet or triplet fragment cluster, respectively. ^{1}O is more reactive than ^{3}O, though either could subsequently drive further intracluster reactions. If ^{3}O is formed, presumably via singlet fission mechanism,[77] a triplet cluster fragment is left behind that is likely much more reactive than a singlet cluster fragment, potentially resulting in intracluster reactions either directly or by release of internal energy upon intersystem crossing back to the singlet state. Since these experiments do not provide direct evidence of the spin states, we performed several quantum chemical calculations comparing singlet and triplet cluster energies for our smallest cluster $(I_2O_5)(IO_3^-)$. Our goal was simply to determine the energetic ordering of the spin channels and whether one or both were energetically available at atmospherically-relevant wavelengths.

We removed O atoms at each unique site and optimized the geometry of the remaining cluster in both the singlet and triplet states. The energy of $(I_2O_5)(IO_3^-)$ was subtracted from the sum of the energies of the corresponding singlet or triplet O atom and remaining cluster, yielding the theoretical onset energy of O loss photofragmentation via the singlet or triplet channel. Since these are open-shell calculations, they were performed at two levels of theory: unrestricted open shell and restricted- open shell. Reported computed

energy differences for each level of theory are displayed in Tables S1 and S2 respectively. We find that both approaches provide similar results, with the ^{1}O loss channels requiring approximately 5.29-5.47 eV of energy and the ^{3}O loss channels only requiring 3.43-4.39 eV of energy to facilitate O loss. At the photon energies in this experiment of 3.65-4.27 eV (290-340 nm), these calculations suggest that it is energetically impossible to access the ^{1}O + ^{1}(cluster). Therefore, we assign photolysis of these clusters to a mechanism resulting in production of an ^{3}O fragment and a ^{3}(cluster).

From these results we can draw some broader inferences about the role of photochemistry in laboratory and ambient NPF studies. First, it is clear that the photoproducts resulting from UV absorption will depend substantially on the power spectrum of the excitation light source, particularly in the region near 300 nm where these clusters begin to absorb significantly. Narrowband laser-like sources, particularly deeper in the non-atmospherically-relevant UV region, may drive non-atmospherically-relevant relative yields of photofragments. Even broadband light sources that do not closely mirror the solar spectrum may induce significant deviations from the ambient abundances of similar clusters due to the sharp turn on of absorption near the atmospheric window. Promotion of the O loss fragmentation channel, in particular, will change the chemical composition of the particle, namely the I:O ratio, while loss of I_2O_5 can be viewed more simply as suppressing growth. Second, even for new particles of only a few nanometers in relatively pristine environments, particle composition is likely to include bases or organics.[78] The fact that fragmentation can yield ^{3}O atoms and ^{3}(cluster) suggests that photoinduced intraparticle chemistry may be common and may play an important role in the fate of new particles containing iodine. Finally, coupling between organic and iodine oxide/iodic acid components of new particles may qualitatively perturb their spectra, borrowing intensity from the strong absorption of the iodine oxides but red shifting their spectra further into the atmospherically relevant range. In this case, the role of photochemistry in new particle evolution would likely be even more pronounced.

In summary, we have found that clusters of the $(I_2O_5)_n(IO_3^-)$ family photofragment by

loss of O, I_2O_5, and I_2O_4. Clusters of increasing size appear to absorb progressively more in the atmospherically relevant region of the UV as they grow, with the larger clusters studied here absorbing up to 340 nm. We also identified the presence of $I_3O_8^-$ in all of the clusters studied using IR spectroscopy, and ultimately identified the cluster chromophore to be $I_3O_8^-$ rather than IO_3^-. Photolysis resulting in loss of I_2O_5 is roughly 10 times faster than O loss fragmentation. O loss likely results in $^3O + {}^3$(cluster), hence intra-cluster chemical reactions are likely to ensue for more complex mixed-composition clusters containing organics. The rich photochemistry of iodine oxide-containing clusters may play a significant role in iodine-based NPF.

Experimental Methods

All mass spectra, IR spectra, and UV spectra discussed in this work were collected on a home-built guided ion beam/ion trap/tandem time-of-flight (TOF) photofragmentation mass spectrometer discussed in detail previously.[11] The anionic clusters analyzed here are formed via electrospray ionization (ESI) of a solution of 5 mM iodic acid in 50/50 water/methanol into an atmospherically-isolated capsule region. The ions are then guided to a cryogenically cooled octopole ion trap (cooled by Sumitomo RDK-408D2 cold head), where they are collisionally cooled with pulsed helium gas. For the mass spectra and UV spectra in Figures 1 and 2, this trap remained at 300K. A laser beam path bisects the trap longitudinally, following the trajectory of the ions. The ions are then orthogonally accelerated and analyzed by time of flight (TOF) mass spectrometry. Tunable UV light was produced by two custom-built optical parametric oscillator (OPO) (LaserVision), which was pumped with 1064nm pump light at a 10 Hz repetition rate, produced by a Nd:YAG laser (Continuum Surelite EX). The signal of the OPO was doubled, yielding the scannable range of 250-340 nm.

For spectra displayed in Figure 3, UV light was generated through sum frequency generation (SFG) of the signal from a similar tunable OPO and the 1064 nm pump light produced by another Continuum Surelite EX laser. Ions were mass selected in the TOF and irradiated at at the space focus of the linear stage of the TOF. A reflectron was used to mass separate

the photofragments from the non-fragmented ions.

The IR spectra were collected at the TOF laser crossing, where tunable IR laser light was produced by an OPO/OPA system (LaserVision) pumped by another Surelite EX. The main difference between the collection processes of the UV and IR spectra results from the CIVP messenger tagging process. For collection of UV spectra, no messenger tags were used.

IR spectra were computed from the ratio of untagged ions to the sum of tagged and untagged ions multiplied by laser power, as a function of wavelength. UV spectra displayed in Figure 1, were computed by dividing the integrated intensity of fragment ions by the sum of the integrated intensity of fragment and parent ions and then divided by the measured laser pulse energy. UV spectra reported in Figure 3 are recorded by monitoring the photofragment only, as it is not possible for the reflectron to focus both fragment and parent ions simultaneously for all fragments due to their kinetic energy differences. This reduction in kinetic energy also results in reduced detection efficiency of the fragments. A method to correct for this effect is described in the Supplementary Information.

Density functional theory calculations were performed at the CAM-B3LYP level of theory, with a split basis set of aug-cc-pVDZ on light atoms and Def2-SV(P) on iodine for all closed shell calculations, using the Gaussian 16 suite of programs.[79] This approach was previously validated for clusters of similar compositions.[74] All open shell calculations were performed using the same basis sets, however, we used both UCAM-B3LYP and ROCAM-B3LYP levels of theory to compare results. All spectra from harmonic frequency calculations are presented without scaling, and all relative energies include zero-point energy.

Acknowledgement

This material is based upon work supported by the National Science Foundation under grant numbers CHE-1905172 and CHE-2215900. Any opinions, findings, and conclusions or recommendations expressed in this material are those of the author(s) and do not necessarily

reflect the views of the National Science Foundation.

Supporting Information Available

The Supporting Information contains additional experimental spectra comparisons, collision induced dissociation mass spectra, and details on how rates were calculated. Further information on singlet versus triplet calculations, adiabatic detachment energy calculations, detection efficiency correction factors, and coordinates for all of the computed clusters are also reported.

References

(1) Merikanto, J.; Spracklen, D.; Mann, G.; Pickering, S.; Carslaw, K. Impact of nucleation on global CCN. *Atmospheric Chemistry and Physics* **2009**, *9*, 8601–8616.

(2) Kulmala, M. et al. Toward direct measurement of atmospheric nucleation. *Science* **2007**, *318*, 89–92.

(3) Lehtipalo, K. et al. The effect of acid–base clustering and ions on the growth of atmospheric nano-particles. *Nature Communications* **2016**, *7*, 1–9.

(4) Kulmala, M.; Maso, M. D.; Mäkelä, J.; Pirjola, L.; Väkevä, M.; Aalto, P.; Miikkulainen, P.; Hämeri, K.; O'dowd, C. On the formation, growth and composition of nucleation mode particles. *Tellus B* **2001**, *53*, 479–490.

(5) Pierce, J.; Adams, P. Uncertainty in global CCN concentrations from uncertain aerosol nucleation and primary emission rates. *Atmospheric Chemistry and Physics* **2009**, *9*, 1339–1356.

(6) Johnson, C. J.; Johnson, M. A. Vibrational spectra and fragmentation pathways of

size-selected, D_2-tagged ammonium/methylammonium bisulfate clusters. *The Journal of Physical Chemistry A* **2013**, *117*, 13265–13274.

(7) Jen, C. N.; McMurry, P. H.; Hanson, D. R. Stabilization of sulfuric acid dimers by ammonia, methylamine, dimethylamine, and trimethylamine. *Journal of Geophysical Research: Atmospheres* **2014**, *119*, 7502–7514.

(8) Temelso, B.; Morrison, E. F.; Speer, D. L.; Cao, B. C.; Appiah-Padi, N.; Kim, G.; Shields, G. C. Effect of mixing ammonia and alkylamines on sulfate aerosol formation. *The Journal of Physical Chemistry A* **2018**, *122*, 1612–1622.

(9) Waller, S. E.; Yang, Y.; Castracane, E.; Racow, E. E.; Kreinbihl, J. J.; Nickson, K. A.; Johnson, C. J. The interplay between hydrogen bonding and coulombic forces in determining the structure of sulfuric acid-amine clusters. *The Journal of Physical Chemistry Letters* **2018**, *9*, 1216–1222.

(10) Yang, Y.; Waller, S. E.; Kreinbihl, J. J.; Johnson, C. J. Direct link between structure and hydration in ammonium and aminium bisulfate clusters implicated in atmospheric new particle formation. *The Journal of Physical Chemistry Letters* **2018**, *9*, 5647–5652.

(11) Waller, S. E.; Yang, Y.; Castracane, E.; Kreinbihl, J. J.; Nickson, K. A.; Johnson, C. J. Electrospray Ionization–Based Synthesis and Validation of Amine-Sulfuric Acid Clusters of Relevance to Atmospheric New Particle Formation. *Journal of The American Society for Mass Spectrometry* **2019**, *30*, 2267–2277.

(12) Yang, Y.; Johnson, C. J. Hydration motifs of ammonium bisulfate clusters of relevance to atmospheric new particle formation. *Faraday Discussions* **2019**, *217*, 47–66.

(13) Kreinbihl, J. J.; Frederiks, N. C.; Waller, S. E.; Yang, Y.; Johnson, C. J. Establishing the structural motifs present in small ammonium and aminium bisulfate clusters of relevance to atmospheric new particle formation. *The Journal of Chemical Physics* **2020**, *153*, 034307.

(14) Kreinbihl, J. J.; Frederiks, N. C.; Johnson, C. J. Hydration motifs of ammonium bisulfate clusters show complex temperature dependence. *The Journal of Chemical Physics* **2021**, *154*, 014304.

(15) Weiss, R. E.; Larson, T. V.; Waggoner, A. P. In situ rapid-response measurement of sulfuric acid/ammonium sulfate aerosols in rural Virginia. *Environmental Science & Technology* **1982**, *16*, 525–532.

(16) Yamato, M.; Iwasaka, Y.; Qian, G.-W.; Ono, A.; Yamanouchi, T.; Sumi, A. Sulfuric acid particles and their neutralization by ammonia in the marine atmosphere: Measurements during cruise from Japan to Antarctica. **1989**, *2*, 29–40.

(17) Erupe, M. E.; Benson, D. R.; Li, J.; Young, L.-H.; Verheggen, B.; Al-Refai, M.; Tahboub, O.; Cunningham, V.; Frimpong, F.; Viggiano, A. A.; Lee, S.-H. Correlation of aerosol nucleation rate with sulfuric acid and ammonia in Kent, Ohio: An atmospheric observation. *Journal of Geophysical Research: Atmospheres* **2010**, *115*.

(18) Kulmala, M.; Petäjä, T.; Ehn, M.; Thornton, J.; Sipilä, M.; Worsnop, D.; Kerminen, V.-M. Chemistry of atmospheric nucleation: on the recent advances on precursor characterization and atmospheric cluster composition in connection with atmospheric new particle formation. *Annual Review of Physical Chemistry* **2014**, *65*, 21–37.

(19) Baek, B. H.; Aneja, V. P. Measurement and analysis of the relationship between ammonia, acid gases, and fine particles in eastern North Carolina. *Journal of the Air & Waste Management Association* **2004**, *54*, 623–633.

(20) Carpenter, L.; Sturges, W.; Penkett, S.; Liss, P.; Alicke, B.; Hebestreit, K.; Platt, U. Short-lived alkyl iodides and bromides at Mace Head, Ireland: Links to biogenic sources and halogen oxide production. *Journal of Geophysical Research: Atmospheres* **1999**, *104*, 1679–1689.

(21) Alicke, B.; Hebestreit, K.; Stutz, J.; Platt, U. Iodine oxide in the marine boundary layer. *Nature* **1999**, *397*, 572–573.

(22) Allan, B. J.; McFiggans, G.; Plane, J. M.; Coe, H. Observations of iodine monoxide in the remote marine boundary layer. *Journal of Geophysical Research: Atmospheres* **2000**, *105*, 14363–14369.

(23) O'Dowd, C. D.; Jimenez, J. L.; Bahreini, R.; Flagan, R. C.; Seinfeld, J. H.; Hämeri, K.; Pirjola, L.; Kulmala, M.; Jennings, S. G.; Hoffmann, T. Marine aerosol formation from biogenic iodine emissions. *Nature* **2002**, *417*, 632–636.

(24) Gómez Martín, J. C.; Mahajan, A. S.; Hay, T. D.; Prados-Román, C.; Ordóñez, C.; MacDonald, S. M.; Plane, J. M.; Sorribas, M.; Gil, M.; Paredes Mora, J. F.; Agama Reyes, M. V.; Oram, D. E.; Leedham, E.; Saiz-Lopez, A. Iodine chemistry in the eastern Pacific marine boundary layer. *Journal of Geophysical Research: Atmospheres* **2013**, *118*, 887–904.

(25) Giese, B.; Laturnus, F.; Adams, F. C.; Wiencke, C. Release of volatile iodinated C_1- C_4 hydrocarbons by marine macroalgae from various climate zones. *Environmental science & technology* **1999**, *33*, 2432–2439.

(26) Thorenz, U. R.; Carpenter, L.; Huang, R.-J.; Kundel, M.; Bosle, J.; Hoffmann, T. Emission of iodine-containing volatiles by selected microalgae species. *Atmospheric Chemistry and Physics* **2014**, *14*, 13327–13335.

(27) Laturnus, F. Volatile halocarbons released from Arctic macroalgae. *Marine Chemistry* **1996**, *55*, 359–366.

(28) Mäkelä, J.; Hoffmann, T.; Holzke, C.; Väkevä, M.; Suni, T.; Mattila, T.; Aalto, P.; Tapper, U.; Kauppinen, E. I.; O'Dowd, C. Biogenic iodine emissions and identification of end-products in coastal ultrafine particles during nucleation bursts. *Journal of Geophysical Research: Atmospheres* **2002**, *107*, PAR–14.

(29) Jimenez, J. L.; Bahreini, R.; Cocker III, D. R.; Zhuang, H.; Varutbangkul, V.; Flagan, R. C.; Seinfeld, J. H.; O'Dowd, C. D.; Hoffmann, T. New particle formation from photooxidation of diiodomethane (CH_2I_2). *Journal of Geophysical Research: Atmospheres* **2003**, *108*, 4318.

(30) Atkinson, H. M.; Huang, R.-J.; Chance, R.; Roscoe, H. K.; Hughes, C.; Davison, B.; Schönhardt, A.; Mahajan, A. S.; Saiz-Lopez, A.; Hoffmann, T.; Liss, P. S. Iodine emissions from the sea ice of the Weddell Sea. *Atmospheric Chemistry and Physics* **2012**, *12*, 11229–11244.

(31) Saiz-Lopez, A.; Plane, J. M. Novel iodine chemistry in the marine boundary layer. *Geophysical Research Letters* **2004**, *31*, L04112.

(32) Leigh, R. J.; Ball, S. M.; Whitehead, J.; Leblanc, C.; Shillings, A. J. L.; Mahajan, A. S.; Oetjen, H.; Lee, J. D.; Jones, C. E.; Dorsey, J. R.; Gallagher, M.; Jones, R. L.; Plane, J. M. C.; Potin, P.; McFiggans, G. Measurements and modelling of molecular iodine emissions, transport and photodestruction in the coastal region around Roscoff. *Atmospheric Chemistry and Physics* **2010**, *10*, 11823–11838.

(33) Garland, J.; Curtis, H. Emission of iodine from the sea surface in the presence of ozone. *Journal of Geophysical Research: Oceans* **1981**, *86*, 3183–3186.

(34) Carpenter, L. J.; MacDonald, S. M.; Shaw, M. D.; Kumar, R.; Saunders, R. W.; Parthipan, R.; Wilson, J.; Plane, J. Atmospheric iodine levels influenced by sea surface emissions of inorganic iodine. *Nature Geoscience* **2013**, *6*, 108–111.

(35) MacDonald, S.; Gómez Martín, J.; Chance, R.; Warriner, S.; Saiz-Lopez, A.; Carpenter, L.; Plane, J. A laboratory characterisation of inorganic iodine emissions from the sea surface: dependence on oceanic variables and parameterisation for global modelling. *Atmospheric Chemistry and Physics* **2014**, *14*, 5841–5852.

(36) Cuevas, C. A.; Maffezzoli, N.; Corella, J. P.; Spolaor, A.; Vallelonga, P.; Kjær, H. A.; Simonsen, M.; Winstrup, M.; Vinther, B.; Horvat, C.; Fernandez, R. P.; Kinnison, D.; Lamarque, J.-F.; Barbante, C.; Saiz-Lopez, A. Rapid increase in atmospheric iodine levels in the North Atlantic since the mid-20th century. *Nature communications* **2018**, *9*, 1452.

(37) Spolaor, A.; Vallelonga, P.; Gabrieli, J.; Kehrwald, N.; Turetta, C.; Cozzi, G.; Poto, L.; Plane, J. M.; Boutron, C.; Barbante, C. Speciation analysis of iodine and bromine at picogram-per-gram levels in polar ice. *Analytical and bioanalytical chemistry* **2013**, *405*, 647–654.

(38) Raso, A. R.; Custard, K. D.; May, N. W.; Tanner, D.; Newburn, M. K.; Walker, L.; Moore, R. J.; Huey, L. G.; Alexander, L.; Shepson, P. B.; Pratt, K. A. Active molecular iodine photochemistry in the Arctic. *Proceedings of the National Academy of Sciences* **2017**, *114*, 10053–10058.

(39) Saiz-Lopez, A.; Saunders, R.; Joseph, D.; Ashworth, S.; Plane, J. Absolute absorption cross-section and photolysis rate of I_2. *Atmospheric Chemistry and Physics* **2004**, *4*, 1443–1450.

(40) Martino, M.; Liss, P. S.; Plane, J. M. The photolysis of dihalomethanes in surface seawater. *Environmental science & technology* **2005**, *39*, 7097–7101.

(41) Martino, M.; Liss, P. S.; Plane, J. M. Wavelength-dependence of the photolysis of diiodomethane in seawater. *Geophysical research letters* **2006**, *33*.

(42) Saiz-Lopez, A. et al. Estimating the climate significance of halogen-driven ozone loss in the tropical marine troposphere. *Atmospheric Chemistry and Physics* **2012**, *12*, 3939–3949.

(43) Gómez Martín, J. C.; Spietz, P.; Burrows, J. P. Spectroscopic studies of the I_2/O_3 photochemistry: Part 1: Determination of the absolute absorption cross sections of

iodine oxides of atmospheric relevance. *Journal of Photochemistry and Photobiology A: Chemistry* **2005**, *176*, 15–38.

(44) Thompson, C. et al. Interactions of bromine, chlorine, and iodine photochemistry during ozone depletions in Barrow, Alaska. *Atmospheric Chemistry and Physics* **2015**, *15*, 9651–9679.

(45) Cox, R.; Bloss, W.; Jones, R.; Rowley, D. OIO and the atmospheric cycle of iodine. *Geophysical Research Letters* **1999**, *26*, 1857–1860.

(46) Bhujel, M.; Marshall, D. L.; Maccarone, A. T.; McKinnon, B. I.; Trevitt, A. J.; da Silva, G.; Blanksby, S. J.; Poad, B. L. Gas phase reactions of iodide and bromide anions with ozone: evidence for stepwise and reversible reactions. *Physical Chemistry Chemical Physics* **2020**, *22*, 9982–9989.

(47) Gómez Martín, J. C.; Lewis, T. R.; Blitz, M. A.; Plane, J.; Kumar, M.; Francisco, J. S.; Saiz-Lopez, A. A gas-to-particle conversion mechanism helps to explain atmospheric particle formation through clustering of iodine oxides. *Nature Communications* **2020**, *11*, 1–14.

(48) Davis, D.; Crawford, J.; Liu, S.; McKeen, S.; Bandy, A.; Thornton, D.; Rowland, F.; Blake, D. Potential impact of iodine on tropospheric levels of ozone and other critical oxidants. *Journal of Geophysical Research: Atmospheres* **1996**, *101*, 2135–2147.

(49) McFiggans, G. et al. Iodine-mediated coastal particle formation: an overview of the Reactive Halogens in the Marine Boundary Layer (RHaMBLe) Roscoff coastal study. *Atmospheric Chemistry and Physics* **2010**, *10*, 2975–2999.

(50) McFiggans, G.; Plane, J. M.; Allan, B. J.; Carpenter, L. J.; Coe, H.; O'Dowd, C. A modeling study of iodine chemistry in the marine boundary layer. *Journal of Geophysical Research: Atmospheres* **2000**, *105*, 14371–14385.

(51) Ingham, T.; Cameron, M.; Crowley, J. N. Photodissociation of IO (355 nm) and OIO (532 nm): Quantum Yields for O (^{3}P) and I (^{2}P$_J$) Production. *The Journal of Physical Chemistry A* **2000**, *104*, 8001–8010.

(52) Spietz, P.; Martín, J. C. G.; Burrows, J. P. Spectroscopic studies of the I_2/O_3 photochemistry: Part 2. Improved spectra of iodine oxides and analysis of the IO absorption spectrum. *Journal of Photochemistry and Photobiology A: Chemistry* **2005**, *176*, 50–67.

(53) Mahajan, A. S.; Shaw, M.; Oetjen, H.; Hornsby, K. E.; Carpenter, L. J.; Kaleschke, L.; Tian-Kunze, X.; Lee, J. D.; Moller, S. J.; Edwards, P.; Commane, R.; Ingham, T.; Heard, D. E.; Plane, J. M. Evidence of reactive iodine chemistry in the Arctic boundary layer. *Journal of Geophysical Research: Atmospheres* **2010**, *115*.

(54) Furneaux, K. et al. Measurements of iodine monoxide at a semi polluted coastal location. *Atmospheric Chemistry and Physics* **2010**, *10*, 3645–3663.

(55) McKinnon, B. I.; Marlton, S. J.; Ucur, B.; Bieske, E. J.; Poad, B. L.; Blanksby, S. J.; Trevitt, A. J. Actinic Wavelength Action Spectroscopy of the IO–Reaction Intermediate. *The Journal of Physical Chemistry Letters* **2021**, *12*, 11939–11944.

(56) Ashworth, S. H.; Allan, B. J.; Plane, J. M. High resolution spectroscopy of the OIO radical: Implications for the ozone-depleting potential of iodine. *Geophysical research letters* **2002**, *29*, 95–1.

(57) Joseph, D.; Ashworth, S.; Plane, J. The absorption cross-section and photochemistry of OIO. *Journal of Photochemistry and Photobiology A: Chemistry* **2005**, *176*, 68–77.

(58) Tucceri, M.; Hölscher, D.; Rodriguez, A.; Dillon, T.; Crowley, J. Absorption cross section and photolysis of OIO. *Physical Chemistry Chemical Physics* **2006**, *8*, 834–846.

(59) Gómez Martín, J. C.; Plane, J. M. Determination of the O–IO bond dissociation energy by photofragment excitation spectroscopy. *Chemical Physics Letters* **2009**, *474*, 79–83.

(60) Gómez Martín, J. C.; Ashworth, S. H.; Mahajan, A. S.; Plane, J. M. Photochemistry of OIO: Laboratory study and atmospheric implications. *Geophysical research letters* **2009**, *36*.

(61) Gómez Martín, J. C.; Spietz, P.; Burrows, J. P. Kinetic and mechanistic studies of the I_2/O_3 photochemistry. *The Journal of Physical Chemistry A* **2007**, *111*, 306–320.

(62) Chameides, W.; Davis, D. Iodine: Its possible role in tropospheric photochemistry. *Journal of Geophysical Research: Oceans* **1980**, *85*, 7383–7398.

(63) Cox, R.; Coker, G. Absorption cross section and kinetics of iodine monoxide (IO) in the photolysis of methyl iodide in the presence of ozone. *The Journal of Physical Chemistry* **1983**, *87*, 4478–4484.

(64) Bloss, W. J.; Rowley, D. M.; Cox, R. A.; Jones, R. L. Kinetics and products of the IO self-reaction. *The Journal of Physical Chemistry A* **2001**, *105*, 7840–7854.

(65) Saiz-Lopez, A.; Fernandez, R. P.; Ordóñez, C.; Kinnison, D. E.; Gómez Martín, J.; Lamarque, J.-F.; Tilmes, S. Iodine chemistry in the troposphere and its effect on ozone. *Atmospheric Chemistry and Physics* **2014**, *14*, 13119–13143.

(66) Lewis, T. R.; Gómez Martín, J. C.; Blitz, M. A.; Cuevas, C. A.; Plane, J.; Saiz-Lopez, A. Determination of the absorption cross sections of higher-order iodine oxides at 355 and 532 nm. *Atmospheric Chemistry and Physics* **2020**, *20*, 10865–10887.

(67) Saunders, R.; Kumar, R.; Martín, J. G.; Mahajan, A.; Murray, B.; Plane, J. Studies of the formation and growth of aerosol from molecular iodine precursor. *Zeitschrift für Physikalische Chemie* **2010**, *224*, 1095–1117.

(68) Gómez Martín, J.; Gálvez, O.; Baeza-Romero, M.; Ingham, T.; Plane, J.; Blitz, M. On the mechanism of iodine oxide particle formation. *Physical Chemistry Chemical Physics* **2013**, *15*, 15612–15622.

(69) Saunders, R. W.; Plane, J. M. Formation pathways and composition of iodine oxide ultra-fine particles. *Environmental Chemistry* **2005**, *2*, 299–303.

(70) He, X.-C. et al. Role of iodine oxoacids in atmospheric aerosol nucleation. *Science* **2021**, *371*, 589–595.

(71) Ahonen, L.; Li, C.; Kubecka, J.; Iyer, S.; Vehkamaki, H.; Petäjä, T.; Kulmala, M.; Hogan Jr, C. J. Ion mobility-mass spectrometry of iodine pentoxide–iodic acid hybrid cluster anions in dry and humidified atmospheres. *The Journal of Physical Chemistry Letters* **2019**, *10*, 1935–1941.

(72) Gómez Martín, J. C.; Lewis, T. R.; James, A. D.; Saiz-Lopez, A.; Plane, J. M. Insights into the Chemistry of Iodine New Particle Formation: The Role of Iodine Oxides and the Source of Iodic Acid. *Journal of the American Chemical Society* **2022**, *144*, 9240–9253.

(73) He, X.-C. et al. Iodine oxoacids enhance nucleation of sulfuric acid particles in the atmosphere. *Science* **2023**, *382*, 1308–1314.

(74) Frederiks, N. C.; Heaney, D. D.; Kreinbihl, J. J.; Johnson, C. J. The Competition between Hydrogen, Halogen, and Covalent Bonding in Atmospherically Relevant Ammonium Iodate Clusters. *Journal of the American Chemical Society* **2023**, *145*, 1165–1175.

(75) National Renewable Energy Laboratory: Reference Air Mass 1.5 Spectra. `https://www.nrel.gov/grid/solar-resource/spectra-am1.5.html`, (accessed 2024-03-28).

(76) Wolk, A. B.; Leavitt, C. M.; Garand, E.; Johnson, M. A. Cryogenic ion chemistry and spectroscopy. *Accounts of Chemical Research* **2014**, *47*, 202–210.

(77) Smith, M. B.; Michl, J. Singlet Fission. *Chemical Reviews* **2010**, *110*, 6891–6936.

(78) Huang, R.-J.; Hoffmann, T.; Ovadnevaite, J.; Laaksonen, A.; Kokkola, H.; Xu, W.; Xu, W.; Ceburnis, D.; Zhang, R.; Seinfeld, J. H.; O'Dowd, C. Heterogeneous iodine-

organic chemistry fast-tracks marine new particle formation. *Proceedings of the National Academy of Sciences* **2022**, *119*, e2201729119.

(79) Frisch, M. J. et al. Gaussian 16 Revision A.03. 2016.